Characterization of Divalent Cation Localization in the Minor Groove of the A_nT_n and T_nA_n DNA Sequence Elements by ^{1}H NMR Spectroscopy and Manganese(II)†

Nicholas V. Hud‡ and Juli Feigon*

Department of Chemistry and Biochemistry and Molecular Biology Institute, University of California, 405 Hilgard Avenue, Los Angeles, California 90095-1569

Received February 22, 2002; Revised Manuscript Received May 29, 2002

ABSTRACT: The localization of Mn^{2+} in A-tract DNA has been studied by ^{1}H NMR spectroscopy using a series of self-complementary dodecamer oligonucleotides that contain the sequence motifs A_nT_n and T_nA_n, where $n = 2$, 3, or 4. Mn^{2+} localization in the minor groove is observed for all the sequences that have been studied, with the position and degree of localization being highly sequence-dependent. The site most favored for Mn^{2+} localization in the minor groove is near the 5′-most ApA step for both the T_nA_n and the A_nT_n series. For the T_nA_n series, this results in two closely spaced symmetry-related Mn^{2+} localization sites near the center of each duplex, while for the A_nT_n series, the two symmetry-related sites are separated by as much as one half-helical turn. The degree of Mn^{2+} localization in the minor groove of the T_nA_n series decreases substantially as the AT sequence element is shortened from T_4A_4 to T_2A_2. The A_nT_n series also exhibits length-dependent Mn^{2+} localization; however, the degree of minor groove occupancy by Mn^{2+} is significantly less than that observed for the T_nA_n series. For both A_nT_n and T_nA_n sequences, the 3′-most AH2 resonance is the least broadened of the AH2 resonances. This is consistent with the observation that the minor groove of A-tract DNA narrows in the 5′ to 3′ direction, apparently becoming too narrow after two base pairs for the entry of a fully hydrated divalent cation. The results that are reported illustrate the delicate interplay that exists between DNA nucleotide sequence, minor groove width, and divalent cation localization. The proposed role of cation localization in helical axis bending by A-tracts is also discussed.

During the past several years, experimental and theoretical studies have provided evidence that cation interaction with duplex DNA is a sequence-specific phenomenon (*1*−*14*). This has important implications for the origin of DNA structure and function. For example, the sequence-specific localization of cations would necessarily result in a nonuniform distribution of cations around duplex DNA polymers. This may in turn be the origin of local variations in DNA structure (e.g., groove narrowing and helical axis bending) (*4*−*7*, *15*, *16*). Furthermore, protein binding to DNA is often coupled with the release of cations from DNA (*17*). Thus, the sequence-specific binding of some proteins to DNA could be partially driven by the release of cations from specific DNA sequences. Despite the clear importance of DNA−cation interactions, the sequence-specific nature of monovalent and divalent cation binding to DNA is not fully characterized.

Divalent cation binding sites in the major groove are presently the most extensively studied class of DNA−counterion interactions (*14*). Using the paramagnetic ion Mn^{2+} as a resonance line broadening probe in solution state ^{1}H NMR spectroscopy experiments, Sletten and co-workers found that Mn^{2+} binds in the major groove of duplex DNA at GpG, GpA, and GpT steps (*1*−*3*). Crystallographic studies have also revealed divalent cations bound at these same steps, and at the ApG step as well (*13*, *18*). The divalent cation binding sites in the DNA major groove appear to be principally defined at the dinucleotide level, with an absolute requirement for at least one guanine base (i.e., GpN or NpG).

In previous reports, we demonstrated that AT-rich sequences can also localize monovalent and divalent cations in a sequence-specific manner in the *minor* groove (*5*, *7*). With respect to divalent cations, we found that Mn^{2+} is localized in the minor groove of the sequence elements A_4T_4 and T_4A_4 in the dodecamer duplexes $[d(GCA_4T_4GC)]_2$ and $[d(CGT_4A_4CG)]_2$, respectively. Our initial motivation to explore cation interaction with AT-rich sequences was to experimentally test our hypothesis that cation interaction with DNA A-tracts (i.e., four to eight adenine or thymine residues without a 5′-TpA-3′ step) could be the origin of the anomalous structural properties associated with A-tract DNA (*19*−*22*). The sequences $[d(GCA_4T_4GC)]_2$ and $[d(CGT_4A_4CG)]_2$ were selected for study because DNA polymers containing the sequence element A_4T_4 exhibit properties associated with A-tracts, whereas those containing T_4A_4 do not (*20*, *23*, *24*).

Here we report a more in-depth analysis of Mn^{2+} localization in the minor groove of the sequence elements A_4T_4 and T_4A_4, along with the closely related sequence elements A_3T_3, T_3A_3, A_2T_2, and T_2A_2. All of these sequence elements are

† Supported by Grant GM48123 from the National Institutes of Health to J.F.

* To whom correspondence should be addressed. Telephone: (310) 206-6922. Fax: (310) 825-0982. E-mail: feigon@mbi.ucla.edu.

‡ Present address: School of Chemistry and Biochemistry, Georgia Institute of Technology, Atlanta, GA 30332. Telephone: (404) 385-1162. Fax: (404) 894-2295. E-mail: hud@chemistry.gatech.edu.

10.1021/bi020159j CCC: $22.00
Published on Web 07/10/2002

within dodecamer duplexes and flanked by G·C base pairs. This study reveals that divalent cation localization in the minor groove of AT-rich sequences can be modulated by base pair changes up to three residues away from the cation localization site, changes that likely affect both the width and electrostatic potential of the minor groove. In contrast to the purely AT regions, no appreciable localization of Mn^{2+} in the minor groove is observed in the GC regions of the duplexes that have been studied. The results presented here provide a framework for understanding, and potentially predicting, divalent cation localization in the DNA minor groove in the solution state.

MATERIALS AND METHODS

Sample Preparation. DNA oligonucleotides were synthesized using standard phosphoramidite chemistry on an Applied Biosystems 392 automated DNA synthesizer. After deprotection in aqueous ammonium hydroxide, oligonucleotides were purified of premature termination products by being passed over a 1 m column of Sephadex G-25 resin (Sigma, St. Louis, MO). Following lyophilization, samples were resuspended and brought to pH 6.0 by titration with 0.5 M NaOH. NMR samples were 450 μL in volume, 2.0 mM oligonucleotide strand, and 50 mM NaCl in 99.999% D_2O.

NMR Data Collection. All ^{1}H spectra were acquired on a Bruker DRX 500 instrument at 500 MHz and 283 K. Mn^{2+} titrations were performed by the addition of 1−4 μL of $MnCl_2$ stock solutions in D_2O. Sample volumes were maintained within approximately 2% of 450 μL over the entire course of a titration by reducing the sample volume, when necessary, with limited drying under nitrogen gas. 1D[1] ^{1}H spectra were collected with 8192 points and a sweep with of 5000 Hz. 2D NOESY spectra were collected with 2048 points in F_2 and 512 blocks in F_1, with a sweep width of 5000 Hz in both dimensions.

Data Analysis. Aromatic and deoxyribose protons were assigned from 2D NOESY spectra using standard sequential connectivity assignment procedures (*25*). Line widths of most AH2 proton resonances were determined by fitting a Lorentzian line function to the 1D data processed with 16K points and no FID apodization. The linear dependence of AH2 resonance line widths on the amount of added $MnCl_2$, from 0.25 to 3.0 μM $MnCl_2$, was used to determine the sensitivity of most AH2 resonances to line broadening by Mn^{2+} in units of hertz per micromolar (Hz/μM) $MnCl_2$. Line widths for the H1′ and H4′ proton resonances, and overlapped AH2 resonances, as a function of the amount of added $MnCl_2$ were determined in the direct dimension at half-height from cross-peaks of each resonance in 2D NOESY spectra processed with 8192 points in F_2 and 1024 points in F_1. 2D spectra used for measurements of Mn^{2+}-induced line broadening were from samples containing 0.7, 1.5, 3.0, and 5.0 μM $MnCl_2$. Line widths for resonances in the absence of paramagnetic broadening were measured from a spectrum of each sample in the presence of 0.1 mM EDTA.

[1] Abbreviations: 1D, one-dimensional; 2D, two-dimensional; NOESY, nuclear Overhauser effect spectroscopy; NDB, Nucleic Acid Database; **A_4T_4**, [d(GCA_4T_4GC)]$_2$; **A_3T_3**, [d($CGCA_3T_3GCG$)]$_2$; **A_2T_2**, [d($GCGCA_2T_2GCGC$)]$_2$; **T_4A_4**, [d(CGT_4A_4CG)]$_2$; **T_3A_3**, [d($GCGT_3A_3CGC$)]$_2$; **T_2A_2**, [d($CGCGT_2A_2CGCG$)]$_2$.

RESULTS

Mn^{2+} Broadening of T_4A_4 Minor Groove ^{1}H Resonances. The aromatic regions of two 1D ^{1}H spectra from a $MnCl_2$ titration of the duplex [d(CGT_4A_4CG)]$_2$ (**T_4A_4**) are presented in Figure 1. A comparison of these two spectra reveals that the A7H2 proton of **T_4A_4** is the aromatic proton most sensitive to resonance line broadening by Mn^{2+}. The AH2 proton is in the minor groove, while the other aromatic protons (i.e., AH8, GH8, CH6, and TH6) are in the major groove. The dramatic line broadening of the A7H2 resonance indicates that **T_4A_4** possesses a preferential site for Mn^{2+} localization in the minor groove. The differential broadening of the four AH2 resonances of **T_4A_4** (i.e., A7H2, A8H2, A9H2, and A10H2) also indicates that Mn^{2+} localization is not uniform over the length of the T_4A_4 sequence element (Figure 1A,B).

The deoxyribose H1′ and H4′ proton resonances provide additional information concerning the localization of Mn^{2+} in the minor groove. These resonances are particularly valuable for monitoring Mn^{2+} localization in regions that contain only G·C base pairs, since this base pair lacks nonexchangeable base protons in the minor groove. However, spectral overlap makes it difficult to extract resonance line broadening information from 1D spectra for most H1′ and H4′ protons (and some AH2 resonances). Therefore, the resonance line broadening of these protons was determined by the analysis of cross-peaks in 2D NOESY spectra (Figure 1C−F). The nonuniform broadening exhibited by the H8/H6−H1′ and H1′−H4′ NOE cross-peaks also supports the preferential localization of Mn^{2+} in the minor groove of the **T_4A_4** duplex. We note that the H1′ resonances are less line broadened by Mn^{2+} than the H4′ resonances; therefore, H4′ resonance line widths were measured using H1′−H4′ cross-peaks. Likewise, the aromatic H8/H6 resonances are less line broadened by Mn^{2+} than the H1′ resonances; therefore, the H8/H6−H1′ cross-peaks were used for the measurement of H1′ line widths.

Broadening of the **T_4A_4** AH2 resonances can be detected for a $MnCl_2$ concentration more than 3 orders of magnitude lower than the oligonucleotide concentration, which indicates that Mn^{2+} is in fast exchange between the DNA duplexes and solution. Increasing the concentration of $MnCl_2$ produces a linear increase in the line width of the **T_4A_4** resonances (Figure 2). Thus, the change in line width of a proton resonance as a function of increased $MnCl_2$ concentration is directly proportional to Mn^{2+} occupancy at the binding site. By measurement of the line width of the AH2, H1′, and H4′ resonances at a number of different $MnCl_2$ concentrations (from 0.3 to 5.0 μM $MnCl_2$), it is possible to compare the relative amount of line broadening in units of hertz per micromolar $MnCl_2$ for proton resonances that exhibit a wide range of sensitivity to the presence of Mn^{2+}, both for different protons within a single duplex and for corresponding protons of different sequences (Table 1). No appreciable changes in chemical shift accompanied resonance line broadening by $MnCl_2$ for any of the protons monitored in this study.

A model of the **T_4A_4** duplex is shown in Figure 3 with van der Waals radius spheres representing the AH2, H1′, and H4′ protons, with sphere color indicating the amount of resonance line broadening by Mn^{2+} in Hz/μM $MnCl_2$. This

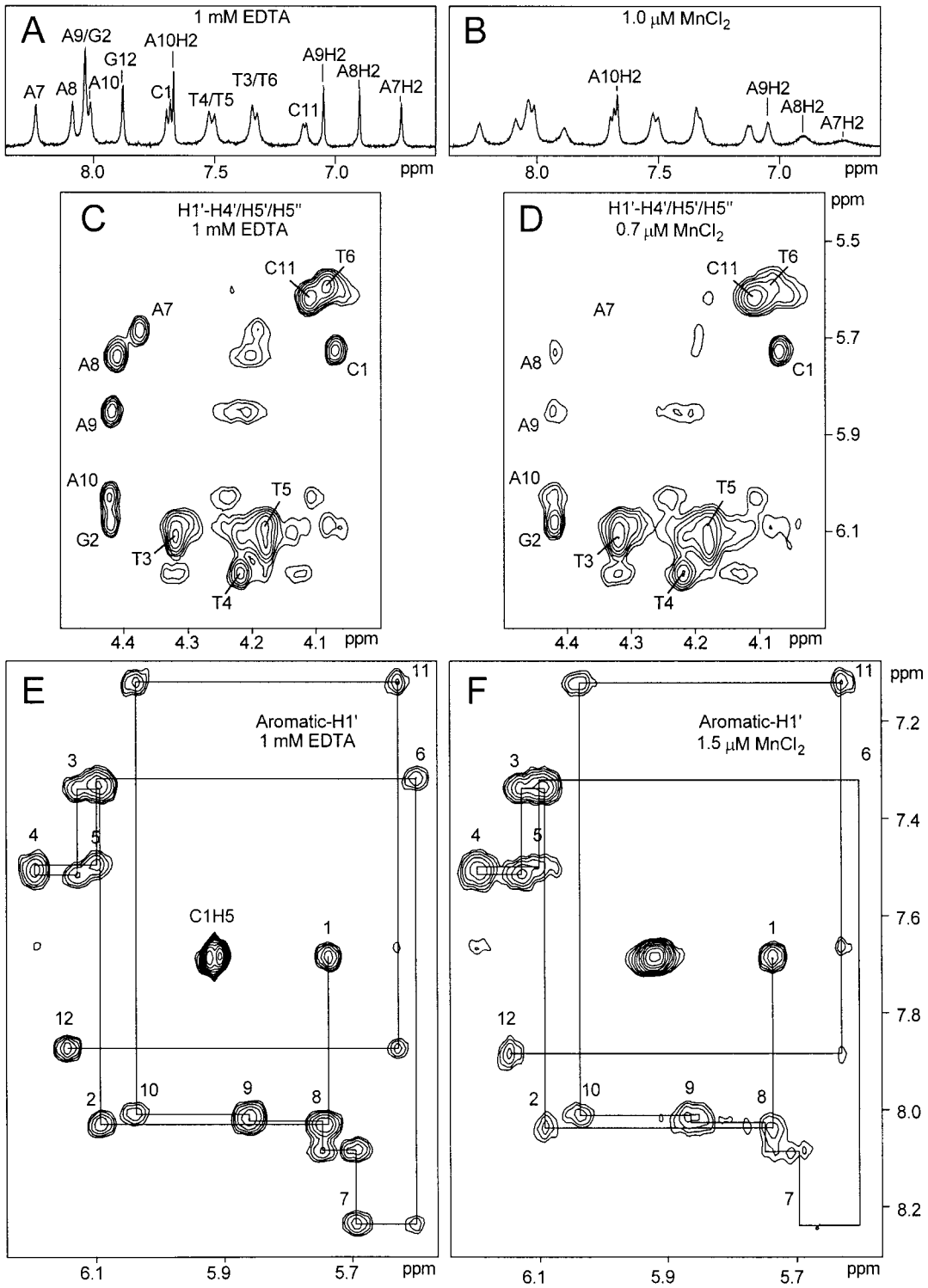

FIGURE 1: (A) Aromatic proton region from the 1D spectrum of $[d(CGT_4A_4CG)]_2$ in the presence of 0.1 mM EDTA. (B) Aromatic proton region from the 1D spectrum of $[d(CGT_4A_4CG)]_2$ in the presence of 1.0 μM $MnCl_2$. (C) H1′−H4′/H5′/H5″ region from a 2D NOESY spectrum of $[d(CGT_4A_4CG)]_2$ in the presence of 0.1 mM EDTA. (D) H1′−H4′/H5′/H5″ region from a 2D NOESY spectrum of $[d(CGT_4A_4CG)]_2$ in the presence of 0.1 μM $MnCl_2$. (E) Aromatic−H1′ region from a 2D NOESY spectrum of $[d(CGT_4A_4CG)]_2$ in the presence of 0.1 mM EDTA. (F) Aromatic−H1′ region from a 2D NOESY spectrum of $[d(CGT_4A_4CG)]_2$ in the presence of 1.5 μM $MnCl_2$. Samples were 2.0 mM in oligonucleotide strand at pH 6.0 with 50 mM NaCl in D_2O. Details about the collection of spectra are given in Materials and Methods.

representation clearly illustrates that the most favored site for Mn^{2+} localization in the minor groove is near the central TpA step. For this duplex, the AH2 and H4′ resonances generally exhibit more line broadening (up to 50 Hz/μM $MnCl_2$) than the H1′ resonances (typically less than 20 Hz/μM $MnCl_2$), even for protons which belong to the same nucleotide residue (Table 1). Since the AH2 protons are on the floor of the minor groove, as opposed to the H4′ protons which are closer to the top of the minor groove, broadening of the AH2 resonances indicates that Mn^{2+} is not merely localized near the phosphates of this groove but is in fact entering deep into the minor groove.

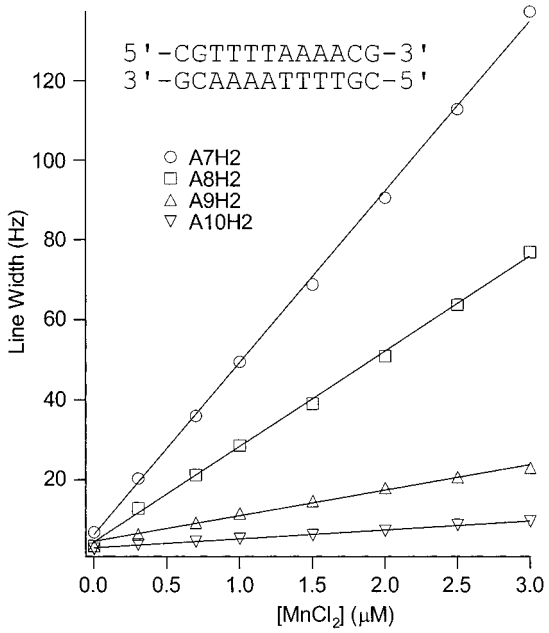

FIGURE 2: Line widths of the AH2 proton resonances of $[d(CGT_4A_4CG)]_2$ as a function of $MnCl_2$ concentration. Samples were 2.0 mM in oligonucleotide strand at pH 6.0 with 50 mM NaCl in D_2O. Line widths were extracted from 1D spectra, such as that shown in Figure 1, by least-squares fits of resonance peaks with Lorentzian line functions.

Table 1: Resonance Line Broadening Susceptibility (Hz/μM $MnCl_2$) for the AH2, H1′, and H4′ Protons of the T_nA_n Series[a]

	$\mathbf{T_4A_4}$			$\mathbf{T_3A_3}$			$\mathbf{T_2A_2}$		
residue	AH2	H1′	H4′	AH2	H1′	H4′	AH2	H1′	H4′
1		0	0		<1	<1		<1	<1
2		1	<1		<1	1		<1	<1
3		<1	1		<1	1		<1	<1
4		4	1		1	<1		2	<1
5		5	*b*		4	2		2	2
6		14	34		11	11		15	10
7	42.5	21	49	26.3	14	21	11.9	13	10
8	25.0	18	48	14.3	14	33	5	18	11
9	6.7	9	28	3	4	18		3	11
10	2.5	5	13		2	7		<1	2
11		<1	<1		<1	1		<1	1
12		<1	<1		<1	<1		<1	<1

[a] Measurements reported to one decimal place are based upon the fitting of a Lorentzian function to the resonance in 1D spectra. [b] Susceptibility to resonance line broadening by Mn^{2+} not determined due to spectral overlap.

The position of a cation binding site on a macromolecule can, in principle, be precisely determined by comparing the relative resonance line broadening of three or more nuclei by a paramagnetic ion (*26*). However, this requires that the contributions of dipolar and scalar coupling to resonance line broadening by the paramagnetic ion be well understood. This is difficult for investigations that utilize Mn^{2+}, since both scalar and dipolar coupling can contribute to resonance line broadening and their relative contributions can depend on several factors (*27*). Furthermore, the precise localization of a cation binding site requires that nuclei used in this determination be sufficiently isolated from the resonance line broadening effects of paramagnetic ions bound at other sites, a criterion that is typically not satisfied for nucleic acids and is definitely not for the molecules of this study (vide infra). This notwithstanding, the resonance line broadenings of A7H2 and A7H4′ by Mn^{2+} (42.5 and 49 Hz/μM $MnCl_2$, respectively) are among the greatest of those measured for the protons of $\mathbf{T_4A_4}$, and therefore, residue A7 is likely near the center of a principle Mn^{2+} binding site. The resonance line broadening measured for A8H2 (25 Hz/μM $MnCl_2$) is also substantial, but reduced in comparison to that of A7H2. This could result from A8H2 being further from the same Mn^{2+} binding site than A7H2. However, the difference in the radial position of a bound Mn^{2+} from protons A7H2 and A8H2 could be very small. For example, if we assume the broadening of both proton resonances results from purely dipolar coupling (which exhibits a distance dependence $\propto r^{-6}$), the difference between the measured line broadening of 25 and 42.5 Hz/μM $MnCl_2$ could result from A8H2 being only a factor of 1.1 further from a Mn^{2+} binding site than A7H2. Given this relationship, a Mn^{2+} binding site near the center of the A7pA8 step would be consistent with the resonance line broadening exhibited by A7H2 and A8H2. This would in turn imply that at least two symmetry-related sites are present in the minor groove of $\mathbf{T_4A_4}$, rather than a single site at the central TpA step, as might be assumed on the basis of a visual inspection of the $\mathbf{T_4A_4}$ duplex in Figure 3.

It is doubtful that any protons near a Mn^{2+} binding site on a DNA duplex are completely isolated from resonance broadening by Mn^{2+} localized at other sites, since the polyanionic nature of DNA produces multiple closely spaced cation localization sites with varying affinities for cations. In the case of $\mathbf{T_4A_4}$, it is clear that Mn^{2+} is in fast exchange between the putative site we have identified at the center of the A7pA8 step and at least one other site on the DNA. This is supported by the measured resonance line broadening of 6.7 Hz/μM $MnCl_2$ for A9H2. If the Mn^{2+} binding site nearest A7H2 were solely responsible for the line broadening of all proton resonances of $\mathbf{T_4A_4}$, then the line broadening of A9H2 should be on the order of 2 Hz/μM $MnCl_2$ (based upon the r^{-6} distance relationship and the broadening measured for A7H2 and A8H2). While these overlapping line broadening effects of neighboring cation localization sites may make it impossible to determine the position of individual Mn^{2+} binding sites to high resolution, resonance line broadening by Mn^{2+} is principally a distance-dependent and occupation-dependent phenomenon. Thus, the preferential localization of divalent cations on a nucleic acid can, in many cases, be sufficiently characterized by the qualitative comparison of resonance line broadening for several nuclei (*28*, *29*). Within this context, we will use our quantitative resonance line broadening measurements for the sequences of this study to interpret the nature of Mn^{2+} interaction with AT-rich DNA, but without attempting to determine the precise location of binding sites in the three-dimensional space around each duplex.

Comparison of the Mn^{+2} Line Broadening of $\mathbf{T_4A_4}$, $\mathbf{T_3A_3}$, and $\mathbf{T_2A_2}$. The localization of Mn^{2+} on the duplexes $[d(GCGT_3A_3CGC)]_2$ ($\mathbf{T_3A_3}$) and $[d(CGCGT_2A_2CGCG)]_2$ ($\mathbf{T_2A_2}$) was also investigated and compared to that of $\mathbf{T_4A_4}$. The sensitivity of the AH2, H1′, and H4′ protons for these two sequences to resonance line broadening by Mn^{2+} is presented in Table 1. For both $\mathbf{T_3A_3}$ and $\mathbf{T_2A_2}$, the magnitude and spatial extent to which Mn^{2+} is localized within the minor groove are decreased with respect to those of $\mathbf{T_4A_4}$ (Figure 3). This is not surprising since A·T base pairs have

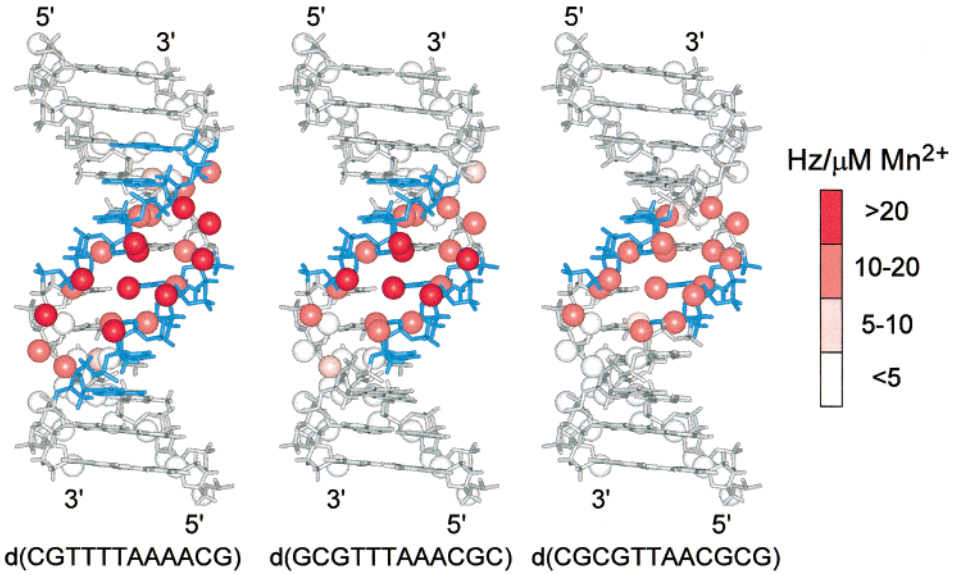

FIGURE 3: Graphic representation of the relative line broadening exhibited by AH2, H1′, and H4′ protons of $[d(CGT_4A_4CG)]_2$, $[d(GCGT_3A_3CGC)]_2$, and $[d(CGCGT_2A_2CGCG)]_2$ as a function of $MnCl_2$ concentration. AH2, H1′, and H4′ protons are represented with van der Waals radius spheres. DNA models shown are based upon idealized coordinates. Line width information was extracted from 1D and 2D NOESY spectra (Materials and Methods).

been replaced with G·C base pairs which are less accommodating to cation binding in the minor groove due to the presence of the guanine N2-amino group (*4*, *30*, *31*). What would have been more difficult to predict is the magnitude of change observed for proton resonance broadening among the three duplexes. For example, A7H2 is part of the TpA step at the center of all four sequences, and has the same nearest neighbor base pairs in all three $\mathbf{T}_n\mathbf{A}_n$ sequences. However, the broadening of this central AH2 clearly depends on the length of the T_nA_n sequence element within which it resides, i.e., 42.5 Hz/μM $MnCl_2$ for $\mathbf{T_4A_4}$, 26.3 Hz/μM $MnCl_2$ for $\mathbf{T_3A_3}$, and 11.9 Hz/μM $MnCl_2$ for $\mathbf{T_2A_2}$ (Figure 4). We note that the reduced resonance line broadening of the A7H2 proton of $\mathbf{T_3A_3}$ by Mn^{2+}, as compared to that of $\mathbf{T_4A_4}$, is the result of a change in nucleotide sequence three nucleotide steps away from the position of this proton. The H1′ and H4′ resonances of $\mathbf{T_3A_3}$ and $\mathbf{T_2A_2}$ show a similar decrease in sensitivity to line broadening by Mn^{2+}, with respect to the corresponding proton resonances of $\mathbf{T_4A_4}$ (Table 1).

Mn^{2+} Broadening of $\mathbf{A_nT_n}$ Minor Groove ^{1}H Resonances. The aromatic region of 1D ^{1}H spectra and selected regions from 2D NOESY spectra for $[d(GCA_4T_4GC)]_2$ ($\mathbf{A_4T_4}$), in the presence of both EDTA and $MnCl_2$, are shown in Figure 5. The 1D spectra demonstrate that AH2 proton line widths, in this case, A3H2 and A4H2, are again the aromatic proton resonances most broadened by Mn^{2+}. A6H2, on the other hand, is one of the least broadened aromatic resonances. The A3H2 and A4H2 resonances exhibit nearly identical line broadening in response to Mn^{2+} (Figure 6), which indicates that localization in the minor groove is most favored at a location equidistant from these two protons (i.e., at the center of the A3pA4 step). This site of Mn^{2+} localization is also supported by line width measurements of H1′ and H4′ (Table 2 and Figure 7). Of these protons, the resonance of T10H4′ shows the most pronounced line broadening by Mn^{2+} of all the resonances of $\mathbf{A_4T_4}$ (Table 2). T10H4′ is located across the minor groove from the A3pA4 step, which is also consistent with the outermost regions of the A-tract being the most favored sites for Mn^{2+} penetration into the $\mathbf{A_4T_4}$ minor groove. On the other hand, the protection of A6H2 from resonance line broadening indicates that Mn^{2+} does not enter the minor groove near the central ApT step.

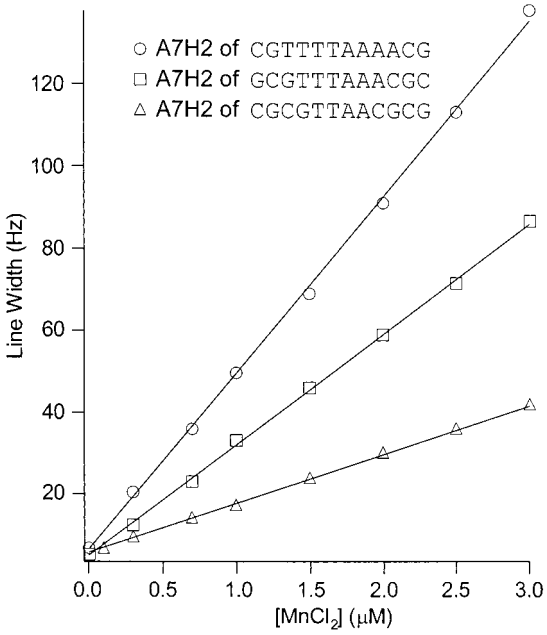

FIGURE 4: Line widths of the central AH2 proton resonances of $[d(CGT_4A_4CG)]_2$, $[d(GCGT_3A_3CGC)]_2$, and $[d(CGCGT_2A_2CGCG)]_2$ as a function of $MnCl_2$ concentration. Samples were 2.0 mM in oligonucleotide strand at pH 6.0 with 50 mM NaCl in D_2O. Line widths were extracted from 1D spectra by least-squares fits of resonance peaks with Lorentzian line functions.

Mn^{2+} resonance line broadening of $\mathbf{A_4T_4}$ minor groove protons is very different from that observed for $\mathbf{T_4A_4}$. First of all, the data for $\mathbf{A_4T_4}$ clearly reveal two symmetry-related sites for minor groove localization that are separated by one-half of a helical turn (Figure 7), whereas $\mathbf{T_4A_4}$ has two closely spaced and centrally located sites (Figure 3). Second, the broadening of the AH2, H1′, and H4′ protons of $\mathbf{A_4T_4}$ is less pronounced and more uniform along the duplex compared to that of $\mathbf{T_4A_4}$. As a specific example, the AH2s of

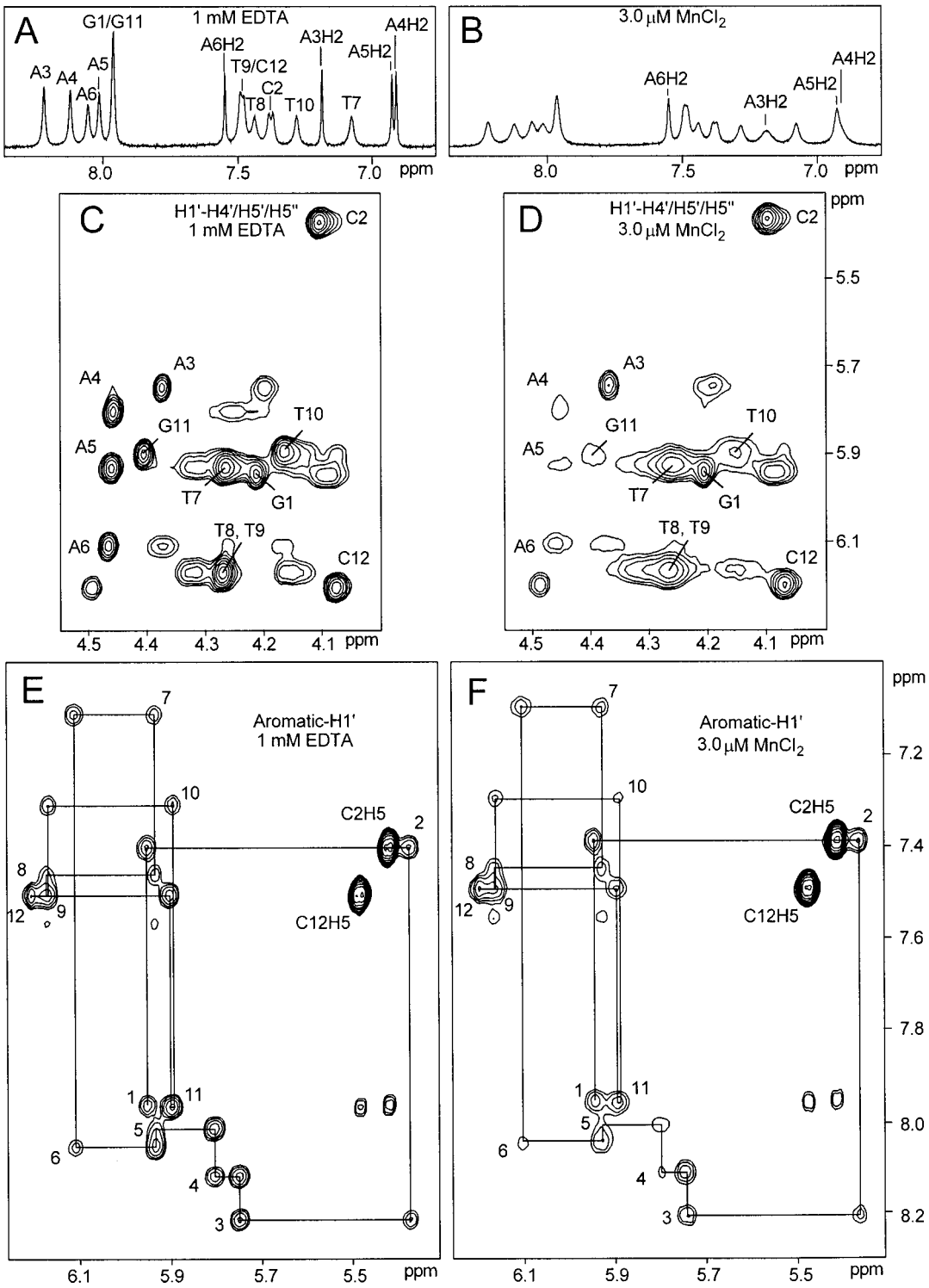

FIGURE 5: (A) Aromatic proton region from the 1D spectrum of $[d(GCA_4T_4GC)]_2$ in the presence of 0.1 mM EDTA. (B) Aromatic proton region from 1D spectrum of $[d(GCA_4T_4GC)]_2$ in the presence of 1.0 μM $MnCl_2$. (C) H1′−H4′/H5′/H5″ region from a 2D NOESY spectrum of $[d(GCA_4T_4GC)]_2$ in the presence of 0.1 mM EDTA. (D) H1′−H4′/H5′/H5″ region from a 2D NOESY spectrum of $[d(GCA_4T_4GC)]_2$ in the presence of 1 μM $MnCl_2$. (E) Aromatic−H1′ region from a 2D NOESY spectrum of $[d(GCA_4T_4GC)]_2$ in the presence of 0.1 mM EDTA. (F) Aromatic−H1′ region from a 2D NOESY spectrum of $[d(GCA_4T_4GC)]_2$ in the presence of 1.5 μM $MnCl_2$. Samples were 2.0 mM in oligonucleotide strand at pH 6.0 with 50 mM NaCl in D_2O. Details about the collection of spectra are given in Materials and Methods.

A_4T_4 exhibit resonance line broadening from 0.9 (A6H2) to 6.7 Hz/μM $MnCl_2$ (A3H2), as compared to a range from 2.5 (A10H2) to 42.5 Hz/μM $MnCl_2$ (A7H2) for **T_4A_4**.

We have also studied the interaction of Mn^{2+} with the duplexes $[d(CGCA_3T_3GCG)]_2$ (**A_3T_3**) and $[d(GCGCA_2T_2GCGC)]_2$ (**A_2T_2**). With regard to AH2 resonance line broadening, **A_3T_3** is very similar to **A_4T_4**. The 5′-most AH2 resonances of these two sequences exhibit a response virtually identical to that of the addition of $MnCl_2$ (Figure 8). This is in contrast to the substantial reduction in AH2 resonance line broadening exhibited by **T_3A_3** in comparison to **T_4A_4**. The shortening of the A_nT_n sequence element from

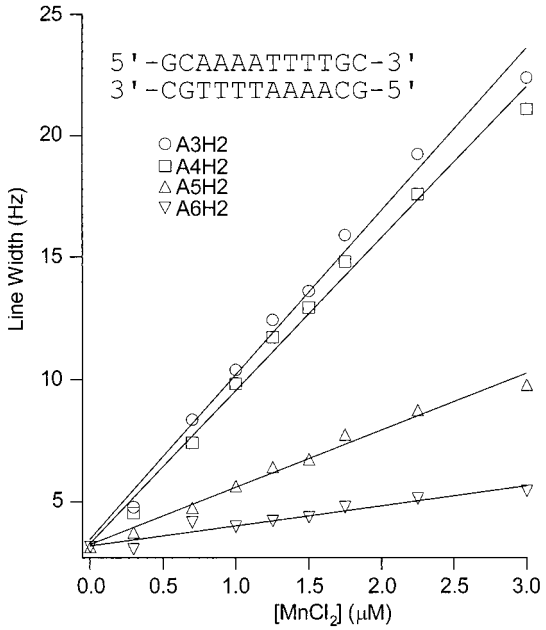

FIGURE 6: Line widths of the AH2 proton resonances of $[d(GCA_4T_4GC)]_2$ as a function of $MnCl_2$ concentration. Samples were 2.0 mM in oligonucleotide strand at pH 6.0 with 50 mM NaCl in D_2O. Line widths were extracted from 1D spectra by least-squares fits of resonance peaks with Lorentzian line functions.

Table 2: Resonance Line Broadening Susceptibility (Hz/μM $MnCl_2$) for the AH2, H1′, and H4′ Protons of the A_nT_n Series[a]

	A_4T_4			**A_3T_3**			**A_2T_2**		
residue	AH2	H1′	H4′	AH2	H1′	H4′	AH2	H1′	H4′
1		<1	<1		<1	<1		<1	<1
2		<1	<1		<1	<1		<1	<1
3	6.7	<1	<1		<1	<1		<1	<1
4	6.3	3	4	7	2	2		<1	1
5	2.4	3	6	6.7	6	9	4.9	2	2
6	0.9	2	6	1	2	9	3	3	4
7		2	4		1	5		2	6
8		1	4		<1	4		3	4
9		2	4		6	5		2	4
10		2	12		3	9		1	*b*
11		2	7		2	4		<1	<1
12		<1	<1		<1	1		<1	<1

[a] Measurements reported to one decimal place are based upon the fitting of a Lorentzian function to the resonance in 1D spectra. [b] Susceptibility to resonance line broadening by Mn^{2+} not determined due to spectral overlap.

A_3T_3 to A_2T_2 does, however, result in an appreciable reduction in the degree of line broadening exhibited by all minor groove protons (Figure 4 and Table 1). For example, the 5′-most AH2 of **A_2T_2** (A5H2) broadens at a rate of 4.9 Hz/μM $MnCl_2$, in comparison to approximately 7 Hz/μM $MnCl_2$ for both **A_4T_4** (A3H2) and **A_3T_3** (A4H2).

Line Broadening of T_nA_n and A_nT_n Major Groove ^{1}H Resonances. Several purine H8 resonances of **T_4A_4** and **A_4T_4** are also affected by the presence of $MnCl_2$ (see the 1D spectra in Figures 1 and 5). These protons reside in the major groove or, arguably, on the border between the major and minor grooves. In the case of **T_4A_4**, the major groove resonances most broadened by Mn^{2+} are G2H8 and G12H8, which broaden at approximately 7 and 5 Hz/μM $MnCl_2$, respectively, and A7H8 and A8H8, which broaden at approximately 5 and 7 Hz/μM $MnCl_2$, respectively. All other H8 and H6 protons of **T_4A_4** exhibit resonance line broadening of <3 Hz/μM $MnCl_2$. The broadening exhibited by G2H8 is not surprising since the dinucleotide step GpT was previously shown to be a favorable divalent cation localization site in the major groove (*32*). The A8H8 and A7H8 protons, on the other hand, belong to an ApA step which, according to a recently reported X-ray crystallography study, does not bind divalent cations in the major groove (*13*). Furthermore, these particular AH8 protons are within 6−10 Å of the most pronounced minor groove Mn^{2+} localization site we have observed (i.e., the 5′-most ApA step of **T_4A_4**). Thus, it is most likely that the resonance line broadening exhibited by the A7H8 and A8H8 protons of **T_4A_4** results from Mn^{2+} being localized on the minor groove side of the same dinucleotide step.

For the **A_nT_n** series, broadening of major groove protons is even less pronounced than for the **T_nA_n** series. The only resonances of **A_4T_4** that are broadened more than 2 Hz/μM $MnCl_2$ are A4H8 (∼2.5 Hz/μM $MnCl_2$) and A5H8 (∼2.5 Hz/μM $MnCl_2$). These resonances are again on the major groove side of the most favored minor groove site for Mn^{2+} localization. Thus, we find no compelling evidence for the sequence-specific localization of Mn^{2+} in the major groove of either the A_nT_n or the T_nA_n sequence elements.

DISCUSSION

Mn^{2+} Localization by T_nA_n and A_nT_n Sequence Elements and the Nature of A-Tract DNA. We have shown by resonance line broadening studies that the most favored site for Mn^{2+} groove localization in a T_nA_n sequence element is in the minor groove at the 5′-most ApA step (or, equivalently, the 3′-most TpT step). AH2 resonance line broadening by Mn^{2+} at this step decreases monotonically as the length of the T_nA_n sequence element is shortened from T_4A_4 to T_2A_2. Furthermore, broadening of the AH2 resonances within T_4A_4 decreases substantially moving from the central A7H2 to the outermost A10H2. Taken together, these results reveal that the two A·T base pairs at the outer edges of T_4A_4 (i.e., A9pA10·T3pT4 in **T_4A_4**) contribute to Mn^{2+} groove localization near the 5′-most ApA step, but do not themselves create a site for Mn^{2+} localization as favorable as the 5′-most ApA step. Our parallel study of the related A_nT_n series also reveals a preference for Mn^{2+} localization in the minor groove at the 5′-most ApA step, and protection of the AH2 resonances of the 3′-most ApA step. However, the interaction of Mn^{2+} with an A_nT_n sequence element is in other ways very different from that observed for the T_nA_n series. First of all, the magnitude of line broadening exhibited is substantially lower for the A_nT_n sequence elements. Second, the effect of sequence length on the magnitude of resonance line broadening is less pronounced for the A_nT_n series than for the T_nA_n series.

The sequence-dependent nature of divalent cation interaction with the A_nT_n and T_nA_n sequence motifs is consistent with the unique structural properties of A-tract DNA. It is well-documented by X-ray crystallography, NMR spectroscopy, and chemical probing that the minor groove of A-tract DNA is narrow compared to that of canonical B-form DNA, and that this narrowing proceeds in the 5′ to 3′ direction along the A-tract minor groove (*5*, *33*−*40*). The anomalous properties of A-tract DNA, such as sequence-directed bending, become appreciable at four or more consecutive A·T base pairs and plateau around eight base pairs (*41*). Another key feature of A-tract DNA is that a 5′-ApT-3′ step does

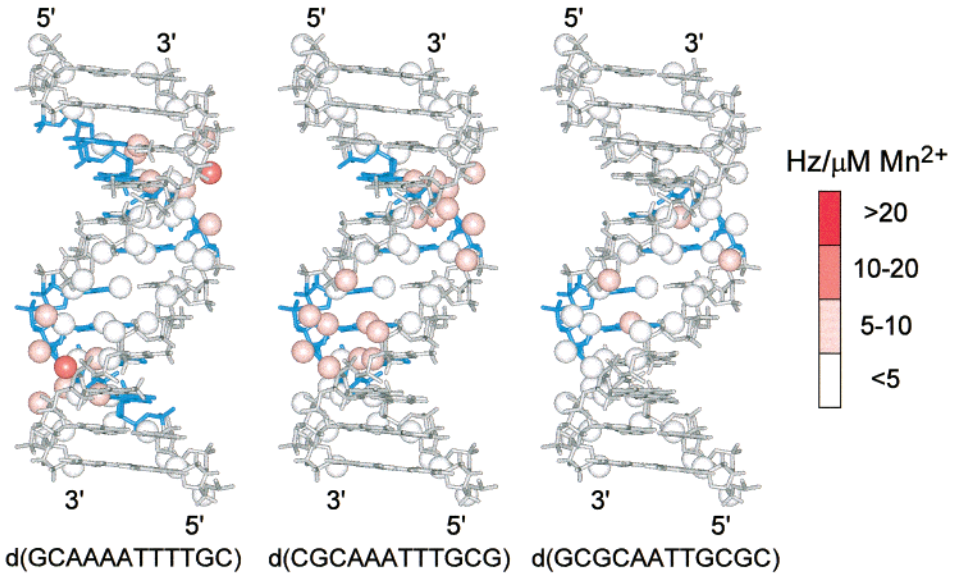

FIGURE 7: Graphic representation of the relative line broadening exhibited by AH2, H1′, and H4′ protons of $[d(GCA_4T_4GC)]_2$, $[d(CGCA_3T_3GCG)]_2$, and $[d(GCGCA_2T_2GCGC)]_2$ as a function of $MnCl_2$ concentration. AH2, H1′, and H4′ protons are represented with van der Waals radius spheres. DNA models shown are based upon idealized coordinates. Line width information was extracted from 1D and 2D NOESY spectra (Materials and Methods).

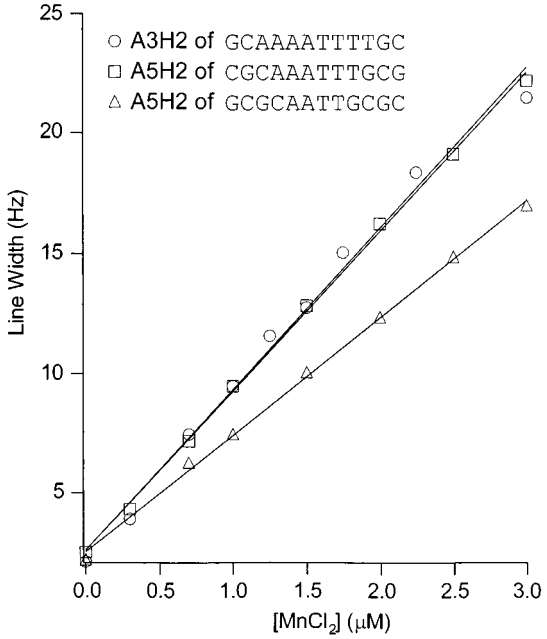

FIGURE 8: Line widths of the outermost AH2 proton resonances of $[d(GCA_4T_4GC)]_2$, $[d(CGCA_3T_3GCG)]_2$, and $[d(GCGCA_2T_2GCGC)]_2$ as a function of $MnCl_2$ concentration. Samples were 2.0 mM in oligonucleotide strand at pH 6.0 with 50 mM NaCl in D_2O. Line widths were extracted from 1D spectra by least-squares fits of resonance peaks with Lorentzian line functions. Note that A5H2 line width data are presented for $[d(CGCA_3T_3GCG)]_2$ in place of A4H2 data since spectral overlap in 1D spectra limited the accuracy of measurements for the line width of A4H2. On the basis of cross-peaks in 2D spectra, the line broadenings of A4H2 and A5H2 of $[d(CGCA_3T_3GCG)]_2$ by Mn^{2+} are identical, within experimental error.

not disrupt an A-tract, with respect to minor groove narrowing and other properties associated with the A-tract, whereas a 5′-TpA-3′ step is apparently completely disruptive to an A-tract (*23*, *41*). Thus, we can view the sequence T_4A_4 as two separate four-base pair A-tracts which are joined at their 5′-ends by a TpA step. Since the 5′-end of an A-tract is wider than the 3′-end, the width of the minor groove at the 5′-most ApA step of T_4A_4 may be optimal for the entry of a fully hydrated Mn^{2+}. In contrast, the lack of evidence for Mn^{2+} penetration into the minor groove at the 3′-end of an A-tract could be the result of the groove becoming too narrow to accommodate a fully hydrated divalent cation. We have previously proposed that this results from the free energy of dehydration being too great for a Mn^{2+} to shed the number of bound water molecules required for entry into a narrow minor groove (*5*). This is consistent with recent X-ray crystal studies which have shown that divalent cations, with a complete inner shell of hydration, enter the minor groove only where this groove is relatively wide (*14*).

The H1′, H4′, and AH2 resonances of $\mathbf{T_3A_3}$ and $\mathbf{T_2A_2}$ are considerably less broadened by Mn^{2+} than their corresponding resonances in $\mathbf{T_4A_4}$, yet the dinucleotide steps identified as the sites of preferential localization are the same for all three sequences in this series. It is possible that the structure of the DNA helix around the Mn^{2+} localization site at the 5′-most ApA step depends on the length of the T_nA_n sequence element. For example, a structural difference near the central TpA step might not favor Mn^{2+} localization as deep in the minor groove as the sequence element is shortened from $\mathbf{T_4A_4}$ to $\mathbf{T_2A_2}$ (e.g., further from the AH2 resonances). However, there is no obvious change in the position of Mn^{2+} binding, as the ratios of line broadening for several resonances near the 5′-most ApA step are very similar for $\mathbf{T_4A_4}$ and $\mathbf{T_3A_3}$. An alternative explanation is that the position of Mn^{2+} localization at the 5′-most ApA step is essentially identical for $\mathbf{T_4A_4}$, $\mathbf{T_3A_3}$, and $\mathbf{T_2A_2}$, but that these sites are simply less occupied for the shorter T_nA_n sequence elements. This lower occupancy could result from the electronegativity of the minor groove being reduced incrementally as the sequence is shortened from $\mathbf{T_4A_4}$ to $\mathbf{T_2A_2}$.

The reduced occupancy of the $\mathbf{A_4T_4}$ minor groove by Mn^{2+} with respect to $\mathbf{T_4A_4}$ is also intriguing. Again, it is possible that the minor groove width of $\mathbf{T_4A_4}$ is more optimal than that of $\mathbf{A_4T_4}$ for accommodating a fully hydrated Mn^{2+} at their respective 5′-most ApA steps. At present, this is difficult

to firmly establish, since the width of the minor groove cannot be determined with high resolution in solution and the minor groove width of DNA duplexes in the crystal state can be affected by crystal packing (*42*) and cation binding (*14*, *18*). Furthermore, it is possible that these differences in cation localization result from differences in both the width and electrostatic potential of the minor groove.

The differences we observe in the relationship between resonance line broadening by Mn^{2+} and sequence length for $\mathbf{A}_n\mathbf{T}_n$ versus $\mathbf{T}_n\mathbf{A}_n$ can also be understood in terms of A-tract structure. As noted above, shortening an A_nT_n sequence element from A_4T_4 to A_3T_3 has little effect on the nature of Mn^{2+} localization (Figures 7 and 8). We can consider the sequence A_4T_4 as an eight-base pair A-tract, since an ApT step is not disruptive to an A-tract. Shortening this sequence to A_3T_3 is then equivalent to shortening an A-tract from eight to six base pairs. A six-base pair A-tract still exhibits the anomalous features of A-tract DNA (e.g., minor groove narrowing). Thus, the outer edges of A_4T_4 and A_3T_3, where Mn^{2+} is most favorably localized in the minor groove, would be very similar for both sequences. In contrast, the central TpA step of the T_nA_n series disrupts properties associated with the A-tract. As discussed above, T_4A_4 is best viewed as two separate four-base pair A-tracts joined at their 5′-ends. Thus, shortening T_4A_4 to T_3A_3 changes the two four-base pair A-tracts of T_4A_4 into two three-base pair "proto A-tracts". Since the anomalous structural properties of A-tract DNA generally become appreciable only at the length of four or more base pairs, the significant reduction observed for the localization of Mn^{2+} by $\mathbf{T_3A_3}$ with respect to $\mathbf{T_4A_4}$ could be the result of the former sequence having substantially muted characteristics of A-tract DNA.

Mn^{2+} Localization in Solution and Divalent Cation Binding Sites in DNA Crystal Structures. Perhaps the most relevant DNA crystal structure presently available for comparison with our solution state results for Mn^{2+} localization on the $\mathbf{T}_n\mathbf{A}_n$ series is the structure of $[d(CGATTAATCG)]_2$ by Quintana et al. (*43*) [Nucleic Acids Database (NDB) ID BDJ031]. $[d(CGATTAATCG)]_2$ contains the sequence element TTAA, making this sequence analogous to $\mathbf{T_2A_2}$. Furthermore, the complete ATTAAT sequence element contains only a single TpA step. Thus, with respect to the definition of A-tract DNA utilized here (i.e., ApT steps do not disrupt an A-tract), ATTAAT is also a reasonable model of $\mathbf{T_3A_3}$ (i.e., both sequences can be viewed as having two three-base pair proto A-tracts joined at their 5′-ends by a TpA step). The crystal structure of $[d(CGATTAATCG)]_2$ contains a single fully hydrated (hexahydrate) Mg^{2+} bound in the minor groove near the central TpA step, where the minor groove is relatively wide (Figure 9). More precisely, the divalent cation is centered at one of the two ApA steps of the duplex, a step that is analogous to the 5′-most ApA step of the $\mathbf{T}_n\mathbf{A}_n$ series. The location of this bound Mg^{2+} is therefore consistent with our determination of the most-favored site for Mn^{2+} localization in the minor groove of the $\mathbf{T}_n\mathbf{A}_n$ series.

The duplex $[d(CGATTAATCG)]_2$ has two symmetry-related A6pA7 steps, yet only one bound cation is observed in the minor groove of the crystal structure. Electrostatic repulsions apparently do not allow two Mg^{2+} ions to simultaneously occupy the two symmetry-related and closely spaced minor groove cation binding sites in the crystal state

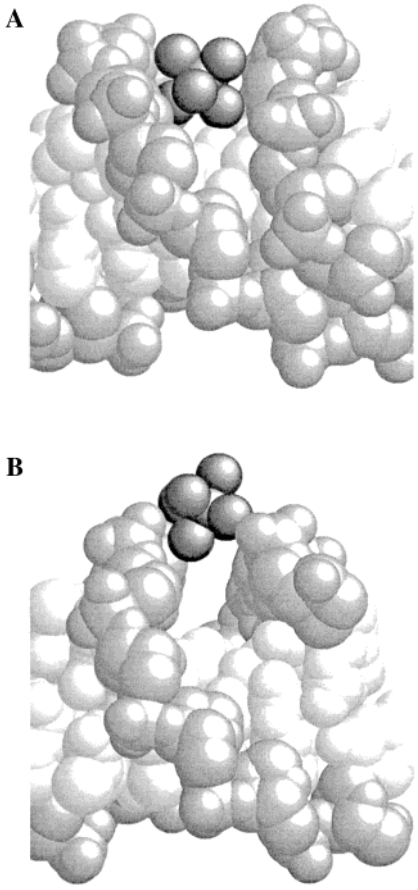

FIGURE 9: (A) Space-filling model of the X-ray crystal structure of $[d(CGATTAATCG)]_2$ with a hexahydrate Mg^{2+} bound in the minor groove (*43*). (B) Space-filling model of the X-ray crystal structure of $[d(CGCGAATTCGCG)]_2$ with a hexahydrate Mg^{2+} bound over the minor groove (*10*).

(*13*, *18*). This is also expected to be the case in the solution state. Furthermore, as mentioned above, our analysis of AH2 line broadening for $\mathbf{T_4A_4}$ revealed that cation localization at the symmetry-related 5′-most ApA steps cannot be the sole source of all AH2 resonance line broadening that is observed. Thus, in contrast to the static bound cation suggested by the X-ray crystal structures, our data indicate that divalent cations in the minor groove of T_nA_n sequences are in fast exchange between the two symmetry-related localization sites at the 5′-most ApA steps and additional sites in the minor groove of lower occupancy.

Several high-resolution structures of the Dickerson dodecamer, d(CGCGAATTCGCG), have recently been reported which provide clear examples of divalent cations bound in the minor groove near an AATT sequence element (*9*, *10*, *44*−*47*). These are arguably the best available crystal structures with which to compare our results from the $\mathbf{A}_n\mathbf{T}_n$ series. In one recently determined crystal structure of the Dickerson dodecamer, a hexahydrate Ca^{2+} was found in the minor groove near the center of the GpA step (*44*) (NDB ID BD0014). Similarly, a hydrated Ca^{2+} was identified at the corresponding location in the structure of the closely related sequence d(GCGAATTCGCG), which forms an 11-base pair helix with a single-base overhang (*9*) (NDB ID BD0018). The ultrahigh-resolution structure of the nonamer d(GCGAATTCG) also contains a hexahydrate Mg^{2+} in the minor groove, but the position of this cation is shifted

approximately one-half of a nucleotide step from the Ca^{2+} binding site into the flanking GC base pairs (NDB ID BD0016) (*45*). We note that the positions of these divalent cation binding sites are at least one nucleotide step removed from what we have identified as the most favored site for Mn^{2+} localization in the minor groove of the $\mathbf{A}_n\mathbf{T}_n$ series (i.e., the 5′-most ApA step). As discussed above, the resonance line broadening for the $\mathbf{A}_n\mathbf{T}_n$ series is less pronounced than that for the $\mathbf{T}_n\mathbf{A}_n$ series. Furthermore, the difference between the broadening of protons along the length of the minor groove of each member of the $\mathbf{A}_n\mathbf{T}_n$ series is also significantly lower in magnitude. This may explain why the results from the crystal structures differ somewhat from our solution state studies. For example, it is possible that upon crystallization changes in hydration result in the preferential binding of divalent cations more toward the GC regions, whereas the binding site for divalent cations in the $\mathbf{T}_n\mathbf{A}_n$ sequence element, being so well-defined, may not be altered as much upon crystallization.

Recent analysis of divalent cations in a number of high-resolution DNA crystal structures has revealed that divalent cations can be bound at the top of a minor groove for DNA sequence elements with a narrow minor groove (e.g., AATT) (*9*, *10*, *46*, *47*). These cations often straddle the two backbones of a minor groove, sharing waters of hydration with the phosphate groups (Figure 9). This is consistent with our proposal that the minor grooves of A-tract sequences become too narrow for the entry of a fully hydrated divalent cation, and that this results in the protection of AH2 resonances in the center of $\mathbf{A_4T_4}$ from line broadening by Mn^{2+}. As an illustration, we estimate that a divalent cation localized above the minor groove of an ApT step would be approximately 9 Å from the AH2 protons of this step. At this distance, we would expect to see essentially no resonance line broadening of AH2 protons as compared to the broadening caused by divalent cations that enter deep into the minor groove (i.e., within 5 Å of an AH2 resonance).

Divalent Cation Localization by A-Tract DNA and the Origin of Sequence-Directed Curvature. We previously proposed that the localization of cations in the minor groove of A-tract DNA results in an asymmetric neutralization of phosphate repulsions around the DNA helix, and that this could in turn be the origin of A-tract-induced helical axis bending (*7*). This hypothesis is supported by the identification of monovalent cation binding sites in the minor groove of A-tract DNA (*7*, *12*, *46*), and by the demonstration that cationic side chains tethered to DNA bases cause bending of the DNA helical axis toward the groove with the tethered cations (*16*, *48*, *49*). The majority of studies concerning the nature of sequence-directed bending by A-tracts are based upon polyacrylamide gel mobility studies carried out in the absence of divalent cations and in the presence of the chelating agent EDTA (*50*). These studies illustrate that divalent cations are not essential for A-tract-induced bending. However, the presence of divalent cations has been shown to at least affect the degree of curvature exhibited by some DNA molecules that contain A-tracts (*51*−*54*). Thus, divalent cation localization must be considered in any complete model of A-tract bending which invokes electrostatic arguments.

We previously identified monovalent cation localization sites in the minor groove of $\mathbf{A_4T_4}$ near the central ApT step, and near the 3′-end of the A-tract in the duplex d(GCAAAAAGC)·d(CGTTTTTGC) (*7*). These sites are perfectly consistent with our model for A-tract helical axis bending since they coincide with the bend centers determined for A-tract DNA using gel mobility studies (*50*). However, divalent cations localized in the minor grooves of A-tract DNA at the sites identified in the present work would not, by themselves, be expected to cause the same helical axis bending characterized by gel mobility experiments since these sites are not located at the bend centers determined for A-tract sequences. In fact, the positions we observe for divalent cation localization in the A-tract minor groove are the converse of those observed for monovalent cation localization. For example, Mn^{2+} localization in the minor groove of $\mathbf{A_4T_4}$ and $\mathbf{T_4A_4}$ is near the 5′-most ApA step of both sequences, whereas the ammonium ion (used as a model of the alkali earth ions) is localized near the 3′-most ApA step of both sequences.

If our model for the origin of A-tract bending by monovalent cations is correct, then one must question why the sites we have identified for divalent cation localization do not predict helical axis bending at locations along A-tract DNA that are known to be A-tract bend centers. One possibility is that divalent cations simply do not cause sequence-directed bending of A-tract DNA in the same manner as monovalent cations. As mentioned above, it has been shown that divalent cations can modulate the curvature of DNA molecules that contain A-tracts (*51*−*54*). However, in gel mobility studies, the non-A-tract sequences that are interspersed with A-tract sequences are frequently G·C-rich (*51*−*53*), and it is known that some G-rich sequences bend toward the major groove in the presence of divalent cations (*55*, *56*). Thus, analysis of A-tract bending in the presence of divalent cations must take into consideration the overall distribution of cations in both DNA grooves. Furthermore, in the narrowest region of an A-tract minor groove, divalent cations may be localized near the top of the groove, rather than deep inside the minor groove, as suggested by X-ray crystallography studies (*46*, *47*). The importance of this latter point is clearly illustrated by a recent study of Maher and co-workers which demonstrates that the precise location of a cation bound in a DNA groove can have a substantial effect on the magnitude of induced helical axis bending (*16*). Therefore, whether an asymmetric distribution of divalent cations contributes to DNA bending in the same way as we postulate for monovalent cations is likely to remain an open question until experiments or theoretical studies are carried out which show explicitly the complete distribution of both divalent and monovalent cations on A-tract sequences.

CONCLUSIONS

The divalent cation Mn^{2+} is localized in a sequence-specific manner within the minor groove of DNA duplexes containing the sequence motifs T_nA_n and A_nT_n. For both sequence motifs, Mn^{2+} localization in the minor groove is favored near the center of the 5′-most ApA step, but Mn^{2+} is apparently restricted from entry into the minor groove near the 3′-most ApA step. As the AT sequence motif is reduced in length from T_4A_4 to T_3A_3 and to T_2A_2 and from A_4T_4 to A_3T_3 and to A_2T_2, the site of most favored Mn^{2+} localization remains near the center of the 5′-most ApA step, but is reduced in relative occupancy as the AT sequence element is shortened. The position we have determined as the most

favored site for Mn^{2+} localization in T_4A_4 coincides with a Mg^{2+} binding site found in the minor groove of the [d(CGATTAATCG)]$_2$ crystal structure. However, resonance line broadening data for minor groove protons cannot be explained by a single bound Mn^{2+}. Thus, in contrast to the crystal structure, our studies reveal a picture of cation localization in the minor groove in which divalent cations rapidly exchange between more than one site with different levels of occupancy.

The results presented here can be summarized into three general conclusions concerning the sequence-specific nature of divalent cation localization within the minor groove of B-form DNA. First of all, a wide and very electronegative minor groove, as found in T_4A_4, provides an excellent site for divalent cation localization. Second, a very electronegative but narrow minor groove, as in A_4T_4, is not nearly as favorable. Third, a wide but amino proton-filled groove, as in GC-rich regions, is not good either. The last principle is in contrast to observations from crystal studies, indicating that divalent cation localization in the GC-rich minor groove may only be favored under the rather extreme dehydrating and molecular crowding conditions of the crystal state. Finally, we note that the results presented here provide further support for our proposal that models for the origin of A-tract sequence-directed curvature must consider the potential effects of asymmetric screening of phosphate−phosphate repulsions by preferentially localized cations.

ACKNOWLEDGMENT

We thank Prof. Frank A. L. Anet for helpful discussions.

REFERENCES

1. Frøystein, N. A., and Sletten, E. (1991) *Acta Chem. Scand. 45*, 219−225.
2. Frøystein, N. A., Davis, J. T., Reid, B. R., and Sletten, E. (1993) *Acta Chem. Scand. 47*, 649−657.
3. Sletten, E., and Frøystein, N. A. (1996) in *Metal Ions in Biological Systems* (Sigel, A., and Sigel, H., Eds.) pp 397−418, Dekker, New York.
4. Young, M. A., Jayaram, B., and Beveridge, D. L. (1997) *J. Am. Chem. Soc. 119*, 59−69.
5. Hud, N. V., and Feigon, J. (1997) *J. Am. Chem. Soc. 119*, 5756−5757.
6. Shui, X. Q., McFail-Isom, L., Hu, G. G., and Williams, L. D. (1998) *Biochemistry 37*, 8341−8355.
7. Hud, N. V., Sklenar, V., and Feigon, J. (1999) *J. Mol. Biol. 286*, 651−660.
8. Feig, M., and Pettitt, B. M. (1999) *Biophys. J. 77*, 1769−1781.
9. Minasov, G., Tereshko, V., and Egli, M. (1999) *J. Mol. Biol. 291*, 83−99.
10. Tereshko, V., Minasov, G., and Egli, M. (1999) *J. Am. Chem. Soc. 121*, 3590−3595.
11. Cheatham, T. E., and Kollman, P. A. (2000) *Annu. Rev. Phys. Chem. 51*, 435−471.
12. Denisov, V. P., and Halle, B. (2000) *Proc. Natl. Acad. Sci. U.S.A. 97*, 629−633.
13. Chiu, T. K., and Dickerson, R. E. (2000) *J. Mol. Biol. 301*, 915−945.
14. Hud, N. V., and Polak, M. (2001) *Curr. Opin. Struct. Biol. 11*, 293−301.
15. McFail-Isom, L., Sines, C. C., and Williams, L. D. (1999) *Curr. Opin. Struct. Biol. 9*, 298−304.
16. Hardwidge, P. R., Lee, D. K., Prakash, T. P., Iglesias, B., Den, R. B., Switzer, C., and Maher, L. J. (2001) *Chem. Biol. 8*, 967−980.
17. Record, M. T., Jr., Zhang, W., and Anderson, C. F. (1998) *Adv. Protein Chem. 51*, 281−353.
18. Kielkopf, C. L., Ding, S., Kuhn, P., and Rees, D. C. (2000) *J. Mol. Biol. 296*, 787−801.
19. Harvey, S. C., Dlakic, M., Griffin, J., Harrington, R., Park, K., Sprous, D., and Sacharias, W. (1995) *J. Biomol. Struct. Dyn. 13*, 301−307.
20. Hagerman, P. J. (1990) *Annu. Rev. Biochem. 59*, 755−781.
21. Dickerson, R. E., Goodsell, D. S., and Neidle, S. A. (1994) *Proc. Natl. Acad. Sci. U.S.A. 91*, 3579−3583.
22. Haran, T. E., Hahn, J. D., and Crothers, D. M. (1994) *J. Mol. Biol. 244*, 135−143.
23. Hagerman, P. J. (1986) *Nature 321*, 449−450.
24. Burkhoff, A. M., and Tullius, T. D. (1987) *Cell 48*, 935−943.
25. Wüthrich, K. (1986) *NMR of Proteins and Nucleic Acids*, John Wiley & Sons, New York.
26. Craik, D. J., and Higging, K. A. (1989) *Annu. Rep. Nucl. Magn. Reson. Spectrosc. 22*, 61−138.
27. Bertini, I., and Luchinat, C. (1986) *NMR of Paramagnetic Molecules in Biological Systems*, pp 319, Benjamin/Cummings Publishing Co., Menlo Park, CA.
28. Allain, F. H.-T., and Varani, G. (1995) *Nucleic Acids Res. 23*, 341−350.
29. Butcher, S. E., Allain, F. H.-T., and Feigon, J. (2000) *Biochemistry 39*, 2174−2182.
30. Lavery, R., and Pullman, B. (1985) *J. Biomol. Struct. Dyn. 2*, 1021−1032.
31. Jayaram, B., Sharp, K. A., and Honig, B. (1989) *Biopolymers 28*, 975−993.
32. Steinkopf, S., and Sletten, E. (1994) *Acta Chem. Scand. 48*, 388−392.
33. Burkhoff, A. M., and Tullius, T. D. (1988) *Nature 331*, 455−457.
34. Katahira, M., Sugeta, H., Kyogoku, Y., Fujii, S., Fujisawa, R., and Tomita, K. (1988) *Nucleic Acids Res. 16*, 8619−8631.
35. Katahira, M., Sueta, H., and Kyogoku, Y. (1990) *Nucleic Acids Res. 18*, 613−618.
36. Nadeau, J. G., and Crothers, D. M. (1989) *Proc. Natl. Acad. Sci. U.S.A. 86*, 2622−2626.
37. Chuprina, V. P., Lipanov, A. A., Federoff, O. Y., Kim, S.-G., Kintanar, A., and Reid, B. R. (1991) *Proc. Natl. Acad. Sci. U.S.A. 88*, 9087−9091.
38. Coll, M., Frederick, C. A., Wang, A. H.-J., and Rich, A. (1987) *Proc. Natl. Acad. Sci. U.S.A. 84*, 8365−8369.
39. Nelson, H. C. M., Finch, J. T., Luisi, B. F., and Klug, A. (1987) *Nature 330*, 221−226.
40. Fratini, A. V., Kopka, M. L., Drew, H., and Dickerson, R. E. (1982) *J. Biol. Chem. 257*, 14686−14707.
41. Koo, H.-S., Wu, H.-M., and Crothers, D. M. (1986) *Nature 320*, 501−506.
42. Lipanov, A., Kopka, M. L., Kaczorgrzeskowiak, M., Quintana, J., and Dickerson, R. E. (1993) *Biochemistry 32*, 1373−1389.
43. Quintana, J. R., Grzeskowiak, K., Yanagi, K., and Dickerson, R. E. (1992) *J. Mol. Biol. 225*, 379−395.
44. Liu, J., and Subirana, J. A. (1999) *J. Biol. Chem. 274*, 24749−24752.
45. Soler-Lopez, M., Malinina, L., Liu, J., Huynh-Dinh, T., and Subirana, J. A. (1999) *J. Biol. Chem. 274*, 23683−23686.
46. Sines, C. C., McFail-Isom, L., Howerton, S. B., Van Derveer, D., and Williams, L. D. (2000) *J. Am. Chem. Soc. 122*, 11048−11056.
47. Tereshko, V., Minasov, G., and Egli, M. (1999) *J. Am. Chem. Soc. 121*, 6970.
48. Strauss, J. K., Prakash, T. P., Roberts, C., Switzer, C., and Maher, L. J. (1996) *Chem. Biol. 3*, 671−678.
49. Strauss, J. K., Roberts, C., Nelson, M. G., Switzer, C., and Maher, L. J. (1996) *Proc. Natl. Acad. Sci. U.S.A. 93*, 9515−9520.
50. Crothers, D. M., and Drak, J. (1992) *Methods Enzymol. 212*, 46−71.
51. Koo, H.-S., Drak, J., Rice, J. A., and Crothers, D. M. (1990) *Biochemistry 29*, 4227−4234.
52. Diekmann, S., and Wang, J. C. (1985) *J. Mol. Biol. 186*, 1−11.
53. Diekmann, S. (1987) *Nucleic Acids Res. 15*, 247−265.
54. Young, M. A., and Beveridge, D. L. (1998) *J. Mol. Biol. 281*, 675−687.
55. Brukner, I., Susic, S., Dlakic, M., Savic, A., and Pongor, S. (1994) *J. Mol. Biol. 236*, 26−32.
56. Rouzina, I., and Bloomfield, V. A. (1998) *Biophys. J. 74*, 3152−3164.

BI020159J